SUPPORTING INFORMATION

Large Second Harmonic Generation and Birefringence from Extended Octupolar π-Conjugated Structures

Danyang Dou,[a] Bingbing Zhang,[a,b] Daqing Yang,[a] and Ying Wang[a,b*]

[a]*College of Chemistry and Materials Science, Key Laboratory of Medicinal Chemistry and Molecular Diagnosis of the Ministry of Education, Hebei Research Center of the Basic Discipline of Synthetic Chemistry, Key Laboratory of Chemical Biology of Hebei Province, Hebei University, Baoding 071002, China*

[b]*Institute of Life Science and Green Development, Hebei University, Baoding 071002, China*

**Corresponding author (Email: wangy@hbu.edu.cn).*

Table of Contents

EXPERIMENTAL AND COMPUTATIONAL METHODS.

Synthesis.

Reagents: Rb_2CO_3 (99%), $CO(NH_2)_2$ (99%), $CsOH·H_2O$ (99.5%) KSCN (99%) and melamine (99.5%) were used as the raw materials. All of them are of analytical grade and were purchased from Aladdin Co, Ltd. without any further treatment.

Synthesis of melon: The melamine was heated in a porcelain crucible at 490 °C for 4 days and the yellow powder melon was synthesized.

Synthesis of $Rb_3[C_6N_7(NCN)_3]·3H_2O$ (**I**):

1. Rb_2CO_3 (0.02 mol) + $CO(NH_2)_2$ (0.04 mol) $\xrightarrow{160\ °C,\ 12h}$ RbCNO (Yield > 95%)

2. RbCNO (10g) + melon (5g) $\xrightarrow{500\ °C,\ 2\ h}$ $Rb_3[C_6N_7(NCN)_3]$ (Yield ~ 66%)

3. $Rb_3[C_6N_7(NCN)_3]$ $\xrightarrow{H_2O}$ $Rb_3[C_6N_7(NCN)_3]·3H_2O$ (Yield ~ 90%)

Synthetic procedure for $Rb_3[C_6N_7(NCN)_3]·3H_2O$ (**I**): Rb_2CO_3 (4.614 g, 0.02 mol) and $CO(NH_2)_2$ (2.4024 g, 0.04 mol) were held at 160 ° C for 24 h to prepare RbCNO. RbCNO (5 g) and melon (10g) were ground evenly and sheated in a ceramic crucible to 500 °C for 2 h, and then turning off the furnace. The product was dissolved in the deionized H_2O (300 mL) and precipitated with triploid volume of anhydrous ethanol. Finally, the white powder was dissolved in deionized water and colorless needle-like crystals of **I** were obtained by slow volatilization of aqueous solution (Figure S4a). IR (cm^{-1}.): O-H: 3368-3465; $[C_6N_7]$ ring: 794, 1183, 1435, 1495, 1643; C≡N: 1495, 2171. Decomposition temperature:350K.

Synthesis of $Cs_3[C_6N_7(NCN)_3]·3H_2O$ (**II**):

1. KSCN (10g) + melon (5g) $\xrightarrow{500\ °C,\ 2\ h}$ $K_3[C_6N_7(NCN)_3]$ (Yield ~ 60%)

2. $K_3[C_6N_7(NCN)_3]$ $\xrightarrow{H_2O}$ $K_3[C_6N_7(NCN)_3]·5H_2O$ (Yield ~ 65%)

3. $K_3[C_6N_7(NCN)_3]·5H_2O$ $\xrightarrow{HCl}$ $H_3[C_6N_7(NCN)_3]$ (Yield > 70%)

4. $H_3[C_6N_7(NCN)_3]$ $\xrightarrow{CsOH·H_2O}$ $Cs_3[C_6N_7(NCN)_3]·3H_2O$ (Yield ~ 80%)

Synthesis procedure for $Cs_3[C_6N_7(NCN)_3]·3H_2O$ (**II**): First, potassium melonate pentahydrate was synthesized as the basis for the subsequent reaction.[1] The melon (8 g) and KSCN (16 g) were ground evenly and slowly heated in a ceramic crucible to 500 °C for 2 h and then turning off the furnace. The product was dissolved in 250 mL water and precipitated with triploid volume of anhydrous ethanol, and the resulting white powder is dissolved in deionized water to obtain potassium melonate pentahydrate. Second, the melonate acid $H_3C_6N_7(NCN)_3$ (b) was precipitated by adding hydrochloric acid to the solution of potassium melonate pentahydrate. The $H_3C_6N_7(NCN)_3$ precipitate was filtered and thoroughly washed three times with deionized water to ensure that no soluble salt was present. Third, the $H_3C_6N_7(NCN)_3$ (5 g) was added to the deionized H_2O (50 mL), and the acidic white suspension was adjusted to neutral with an aqueous solution of CsOH (3 mol/L) and stirred for 2 h. Finally, the solution was used for crystallization using antisolvent diffusion method, while ethanol was selected as the poor solvent. Colorless needle-like crystals of **II** were obtained after two weeks (Figure S4b). IR (cm^{-1}.): O-H: 3460-3436; $[C_6N_7]$ ring: 789, 1183, 1427, 1487, 1639; C≡N: 1487, 2167. Decomposition temperature: 370K.

Single-Crystal X-ray Diffraction (XRD). The single-crystal XRD data were collected by the Bruker D8 VENTURE diffractometer (Mo-Kα radiation, λ = 0.71073 Å). Data integration and absorption corrections were carried out using the *SAINT*[2] program. The single crystal data were analyzed with the *Olex*2 program.[3] The structure was solved using Intrinsic Phasing method,[4] and refined using the least–squares technique on F_o^2 with data having $F_o^2 \geq 2\sigma$ (F_o^2). Solutions were checked for missed symmetry using the PLATON program.[5] The detailed crystal data and structure refinement are listed in Tables S1-S5.

Powder XRD. Dandong Haoyuan DX-27 mini X-ray diffractometer (Cu Kα, λ = 1.5406 Å) was used to collect the XRD data at room temperature. The angular (2θ) range was 10−70° with a scan step width of 0.02° and a fixed counting time of 2 s.

Elemental Analysis. Scanning electronic microscope (SEM) images and Energy Dispersive X-ray (EDX) microanalysis of the crystal were performed on a Hitachi TM4000Plus microscope with an acceleration voltage of 15 kV.

X-ray Photoelectron Spectroscopy (XPS). XPS analysis was performed on a Thermo Scientific K-Alpha spectrometer using a focused monochromatized Al *Kα* radiation (1486.6 eV).

Infrared Spectroscopy. The Infrared spectrum was recorded with a Nicolet iS10 spectrometer in the wavelength of 400-4000 cm^{-1}. A transparent pellet for measurement was prepared by pressing a thoroughly ground mixture of crystal sample and KBr at a ratio of 1:100.

Thermal Analysis. Thermal gravimetric (TG) analysis and differential scanning calorimetry (DSC) were measured on a NETZSCH simultaneous STA 449 F3 thermal analyzer in air, heated from room temperature to 800 °C at a rate of 10 °C min^{-1}.

Ultraviolet-visible−Near-Infrared (UV−Vis−NIR) Diffuse Reflectance Spectroscopy. The diffuse reflectance spectrum was measured with a Shimadzu UV 2600i spectrometer in the 190–1100 nm wavelength range. The reflectance spectra were converted to absorbance using the Kubelka−Munk relation.

Birefringence Tests. The birefringence was measured by interference color method [6] using a NIKON Eclipse Ci-POL polarizing microscope equipped with Berek compensator calibrated at 546 nm. To increase the accuracy, the compensator was tilted in opposite directions (left and right rotation) until the crystal color achieve maximum darkness. The measurement was first performed under while light and further test with monochromatic light using a 546 nm optical filter. The birefringence was calculated according to the following equation: R (retardation) = $\Delta n \times d$, where R represents the optical path difference, Δn is the birefringence, and d denotes the thickness.

Second-Order NLO Measurements. The powder SHG responses were measured by the Kurtz–Perry method[7] with a Q-switched Nd: YAG solid-state laser at 1064 nm (10Hz, 100 μJ). After grinding and sieving, the polycrystalline powder samples were divided into different particle sizes: 20-38.5, 38.5-55, 55-80, 80-125, 125-160, 160-200 and 200-250 μm. The sieved KDP and BBO samples with the same particle ranges were used as a reference. The samples were pressed between glass slides and secured with tape in 1-mm thick aluminum holders that contained an 8-mm diameter hole. Subsequently, they were placed into a light-tight box and irradiated with a laser. The photomultiplier tube collected the intensity of the frequency-doubled output emitted from the samples. No index-matching oil was used during the tests.

Computational Methods. *Ab initio* calculations were conducted by Gaussian 09 program.[8] The structures used for calculations were fully optimized using *B3LYP* functional with *cc-pVDZ* basis

sets. To discuss the optical anisotropy and second-order NLO property of anions system, the polarizability and first hyperpolarizability of the optimized structures were studied with *B3LYP/aug-cc-pVDZ*. The wavefunction analysis was carried out with *Multiwfn* 3.8 (dev) code,[9] and the isosurface graphs were rendered by VMD program.[10] The CASTEP code[11] performed the first-principles calculations. The exchange−correlation energy was described by using Perdew−Burke−Ernzerhof (PBE) functional within the generalized gradient approximation (GGA).[12] The ion-electron interactions were handled with norm-conserving pseudopotentials.[13, 14] The plane-wave energy cutoff and Monkhorst-Pack *k*–point in the Brillouin zone were set at 750.0 eV and 4 × 1 × 2, respectively. Before bandgap and optical property calculation, the atomic positions were fully optimized while cell parameters were fixed. To provide more accurate band gap values, the HSE06 hybrid functional was chosen.[15, 16] Based on the scissor–corrected (1.06 eV and 1.04 eV) electron structure, the linear optical refractive indices, and birefringence can be obtained by the real part of the dielectric function. The NLO properties were calculated based on the length-gauge formalism.[17] At a zero-frequency limit, the static SHG coefficients can be attributed to Virtual-Electron (VE) and Virtual-Hole (VH) processes.[18] To explore the origin of the NLO properties, a SHG-density analysis was employed.[19] This allows for highlighting the origin of SHG optical nonlinearity in real space through the resulting distribution of the densities of each state.

ADDITIONAL TABLES AND FIGURES

Table S1. Crystal data and structure refinement for $M_3[C_6N_7(NCN)_3]\cdot 3H_2O$.

Empirical formula	$Rb_3C_9N_{13}H_6O_3$	$Cs_3C_9N_{13}H_6O_3$
Formula weight	600.68	743.00
Temperature [K]	273(2)	273(2)
Crystal system	orthorhombic	orthorhombic
Space group (number)	$Pna2_1$ (33)	$Pna2_1$ (33)
a [Å]	6.8905(17)	6.898(3)
b [Å]	21.852(5)	21.946(8)
c [Å]	12.298(3)	12.324(3)
Volume [Å^3]	1851.7(8)	1865.7(11)
Z	4	4
ρ_{calc} [gcm^{-3}]	2.155	2.645
μ [mm^{-1}]	7.941	5.874
F(000)	1144	1360
Index ranges	$-8 \le h \le 8$, $-28 \le k \le 28$, $-15 \le l \le 15$	$-8 \le h \le 8$, $-28 \le k \le 28$, $-15 \le l \le 16$
Reflections collected / unique	24051/4248	29969/3267
Completeness	99.6 %	99.8 %
Data / Restraints / Parameters	4248/22/273	3267/22/272
Goodness-of-fit on F^2	1.129	1.084
Final R indexes [$I \ge 2\sigma(I)$][a]	$R_1 = 0.0357$, w$R_2 = 0.0964$	$R_1 = 0.0517$, w$R_2 = 0.1139$
Final R indexes [all data][a]	$R_1 = 0.0388$, w$R_2 = 0.0992$	$R_1 = 0.0692$, w$R_2 = 0.1217$
Largest peak/hole [eÅ^{-3}]	1.30/-0.74	1.66/-0.87
Flack X parameter	0.449(18)	0.13(8)

[a] $R_1 = \Sigma||F_o|-|F_c||/\Sigma|F_o|$ and w$R_2 = [\Sigma w(F_o^2 - F_c^2)^2/\Sigma wF_o^4]^{1/2}$

Table S2. Atomic coordinates and equivalent isotropic displacement parameters for **I**.

Atom	x	y	z	U_{eq}
Rb1	0.67495(11)	0.67053(4)	-0.03141(6)	0.0454(2)
Rb2	0.28835(9)	0.60072(3)	0.29770(6)	0.03466(19)
Rb3	0.31034(9)	0.97075(3)	0.50315(6)	0.0374(2)
N1	0.3671(15)	0.7253(5)	0.1303(8)	0.065(2)
N2	0.4195(12)	0.8005(3)	0.2792(7)	0.0531(18)
N3	0.4588(12)	0.8284(4)	0.4542(6)	0.0488(17)
N4	0.4410(11)	0.7222(4)	0.4059(6)	0.0465(16)
N5	0.4668(12)	0.6488(3)	0.5390(6)	0.0496(17)
N6	0.4784(10)	0.7522(3)	0.5883(6)	0.0401(14)
N7	0.4892(12)	0.8579(3)	0.6313(6)	0.0465(16)
N8	0.5012(15)	0.9902(4)	0.7623(9)	0.064(2)
N9	0.5185(12)	0.8814(3)	0.8147(7)	0.0513(17)
N10	0.5099(11)	0.7801(3)	0.7724(7)	0.0484(17)
N11	0.5005(11)	0.6780(3)	0.7266(7)	0.0474(16)
N12	0.4817(12)	0.5769(4)	0.6708(7)	0.0532(18)
N13	0.5096(15)	0.5419(4)	0.8580(8)	0.066(2)
C1	0.3978(14)	0.7586(4)	0.2045(7)	0.0487(19)
C2	0.4418(12)	0.7824(4)	0.3828(7)	0.0430(18)
C3	0.4746(12)	0.8145(4)	0.5576(7)	0.0404(17)
C4	0.4635(11)	0.7066(4)	0.5086(7)	0.0416(16)
C5	0.4847(12)	0.6363(4)	0.6469(7)	0.0440(18)
C6	0.4980(12)	0.7368(4)	0.6990(8)	0.0437(18)
C7	0.5062(12)	0.8382(4)	0.7384(8)	0.0443(19)
C8	0.5075(14)	0.9384(4)	0.7806(8)	0.051(2)
C9	0.4982(14)	0.5609(4)	0.7735(8)	0.048(2)
O1	1.1667(19)	0.6237(7)	0.0365(13)	0.117(4)
H1A	1.062(19)	0.609(7)	0.071(16)	0.164
H1B	1.17(3)	0.6650(19)	0.03(2)	0.164
O2	0.6992(17)	0.5929(5)	0.2133(12)	0.102(3)
H2A	0.75(2)	0.559(5)	0.183(14)	0.143
H2B	0.585(14)	0.604(7)	0.185(14)	0.143
O3	0.7387(13)	0.9944(5)	0.5196(9)	0.093(3)
H3A	0.851(10)	1.005(8)	0.554(12)	0.130
H3B	0.636(12)	1.015(7)	0.545(12)	0.130

U_{eq} is defined as 1/3 of the trace of the orthogonalized U_{ij} tensor.

Table S3. Atomic coordinates and equivalent isotropic displacement parameters for **II**.

Atom	x	y	z	U_{eq}
Cs1	0.3235(2)	0.32930(8)	0.43573(11)	0.0512(5)
Cs2	0.71228(19)	0.39966(6)	-0.23514(11)	0.0396(4)
Cs3	0.6893(2)	0.02941(6)	-0.02991(11)	0.0419(4)
N1	0.483(2)	0.1183(7)	0.2806(14)	0.028(4)
N2	0.498(3)	0.3222(8)	0.1921(14)	0.027(4)
N3	0.485(2)	0.2204(7)	0.2394(14)	0.028(4)
N4	0.522(2)	0.2481(7)	0.0561(13)	0.024(4)
N5	0.512(3)	0.1435(7)	0.1013(14)	0.029(4)
N6	0.522(2)	0.4245(7)	0.1386(15)	0.029(4)
N7	0.531(2)	0.3499(7)	0.0057(13)	0.026(4)
N8	0.558(2)	0.2773(8)	-0.1259(14)	0.027(4)
N9	0.582(3)	0.2007(7)	-0.2541(14)	0.035(4)
N10	0.633(3)	0.2742(9)	-0.4012(15)	0.038(4)
N11	0.498(3)	0.0104(8)	0.2304(17)	0.042(5)
N12	0.488(3)	0.4567(11)	0.3276(16)	0.046(5)
N13	0.542(2)	0.1706(7)	-0.0786(14)	0.026(4)
C1	0.501(3)	0.4395(10)	0.241(2)	0.037(5)
C2	0.502(3)	0.2639(8)	0.1655(16)	0.023(4)
C3	0.490(3)	0.1621(10)	0.2048(17)	0.030(5)
C4	0.526(3)	0.1860(8)	0.0241(16)	0.020(4)
C5	0.514(3)	0.3635(10)	0.1128(19)	0.033(5)
C6	0.535(3)	0.2939(8)	-0.0239(17)	0.026(4)
C7	0.606(3)	0.2418(10)	-0.3281(15)	0.029(5)
C8	0.559(3)	0.2175(10)	-0.1497(15)	0.024(4)
C9	0.492(3)	0.0623(9)	0.2496(18)	0.029(5)
O1	0.762(2)	0.4946(10)	-0.0137(13)	0.061(5)
H1A	0.71(4)	0.461(7)	0.009(18)	0.085
H1B	0.76(4)	0.501(12)	-0.084(5)	0.085
O2	0.834(4)	0.3762(10)	-0.4951(15)	0.081(7)
H2A	0.84(5)	0.370(13)	-0.566(5)	0.113
H2B	0.80(5)	0.345(9)	-0.455(19)	0.113
O3	0.296(3)	0.4060(9)	0.683(3)	0.090(8)
H3A	0.39(4)	0.391(13)	0.64(2)	0.125
H3B	0.24(5)	0.380(12)	0.73(2)	0.125

U_{eq} is defined as 1/3 of the trace of the orthogonalized U_{ij} tensor.

Table S4. Selected bond distances and angles (Å) of **I**.

Atom–Atom	Length [Å]	Atom–Atom	Length [Å]
Rb1–N1	3.144(10)	N1–C1	1.187(13)
Rb1–N11$^{\#1}$	3.214(8)	N2–C1	1.305(12)
Rb1–N9$^{\#2}$	3.236(8)	N2–C2	1.343(12)
Rb1–N1$^{\#3}$	3.300(10)	N3–C3	1.312(11)
Rb1–N13$^{\#1}$	3.325(10)	N3–C2	1.340(12)
Rb1–O2	3.459(14)	N4–C4	1.318(12)
Rb1–N10$^{\#2}$	3.509(8)	N4–C2	1.344(12)
Rb1–N10$^{\#1}$	3.584(8)	N5–C4	1.317(11)
Rb1–O1	3.636(14)	N5–C5	1.360(12)
Rb2–O2	3.020(12)	N6–C4	1.401(11)
Rb2–N4	3.151(8)	N6–C6	1.409(12)
Rb2–N8$^{\#4}$	3.164(9)	N6–C3	1.412(10)
Rb2–N2$^{\#5}$	3.343(8)	N7–C3	1.315(11)
Rb2–N3$^{\#5}$	3.356(8)	N7–C7	1.390(11)
Rb2–O1$^{\#6}$	3.358(16)	N8–C8	1.154(12)
Rb2–N5	3.380(8)	N9–C8	1.318(12)
Rb2–O3$^{\#5}$	3.447(12)	N9–C7	1.334(12)
Rb2–N1	3.455(10)	N10–C6	1.311(12)
Rb2–N13$^{\#7}$	3.492(10)	N10–C7	1.336(12)
Rb3–O3	3.003(10)	N11–C6	1.328(11)
Rb3–N7	3.176(8)	N11–C5	1.343(11)
Rb3–N13$^{\#8}$	3.234(11)	N12–C9	1.315(13)
Rb3–N12$^{\#5}$	3.235(9)	N12–C5	1.332(12)
Rb3–N3	3.330(8)	N13–C9	1.122(13)
Rb3–N8$^{\#9}$	3.345(11)		
Rb3–O1$^{\#10}$	3.371(15)		
Rb3–N8	3.473(11)		
Rb3–N5$^{\#5}$	3.553(8)		

Atom–Atom–Atom	Angle [°]	Atom–Atom–Atom	Angle [°]
C1–N2–C2	118.3(8)	C6–N11–C5	117.9(8)
C3–N3–C2	117.9(8)	C9–N12–C5	118.0(9)
C4–N4–C2	117.1(8)	N1–C1–N2	172.8(11)
C4–N5–C5	118.1(8)	N3–C2–N2	114.2(8)
C4–N6–C6	120.8(7)	N3–C2–N4	126.6(8)
C4–N6–C3	119.8(7)	N2–C2–N4	119.2(8)
C6–N6–C3	119.3(7)	N3–C3–N7	120.5(8)
C3–N7–C7	115.9(8)	N3–C3–N6	118.9(7)
C8–N9–C7	116.2(9)	N7–C3–N6	120.6(8)
C6–N10–C7	118.0(8)	N5–C4–N4	121.5(8)
N5–C4–N6	118.8(8)	N10–C6–N6	119.9(8)
N4–C4–N6	119.6(8)	N11–C6–N6	118.7(8)

N12–C5–N11	120.1(9)	N9–C7–N10	116.8(8)
N12–C5–N5	114.2(8)	N9–C7–N7	117.0(8)
N11–C5–N5	125.7(8)	N10–C7–N7	126.3(8)
N10–C6–N11	121.4(9)	N8–C8–N9	172.6(11)

Symmetry transformations used to generate equivalent atoms:

#1: +X, +Y, -1+Z; #2: 0.5+X, 1.5-Y, -1+Z; #3: 0.5+X, 1.5-Y, +Z; #4: 0.5-X, -0.5+Y, -0.5+Z; #5: -0.5+X, 1.5-Y, +Z; #6: -1+X, +Y, +Z; #7: 1-X, 1-Y, -0.5+Z; #8: 0.5-X, 0.5+Y, -0.5+Z; #9: 1-X, 2-Y, -0.5+Z; #10: 1.5-X, 0.5+Y, 0.5+Z; #11: 0.5-X, 0.5+Y, 0.5+Z; #12: 1-X, 2-Y, 0.5+Z; #13: -0.5+X, 1.5-Y, 1+Z; #14: +X, +Y, 1+Z; #15: 0.5-X, -0.5+Y, 0.5+Z; #16: 1-X, 1-Y, 0.5+Z; #17: 1+X, +Y, +Z; #18: 1.5-X, -0.5+Y, -0.5+Z;

Table S5. Selected bond distances and angles (Å) of **II**.

Atom–Atom	Length [Å]	Atom–Atom	Length [Å]
Cs1–N10$^{\#1}$	3.172(18)	N1–C9	1.29(2)
Cs1–N2	3.238(17)	N1–C3	1.34(3)
Cs1–N1$^{\#2}$	3.242(16)	N2–C2	1.32(2)
Cs1–N12	3.30(2)	N2–C5	1.34(3)
Cs1–N10$^{\#3}$	3.304(19)	N3–C2	1.33(3)
Cs1–O3	3.49(3)	N3–C3	1.35(3)
Cs1–N3$^{\#2}$	3.534(17)	N4–C2	1.40(3)
Cs1–N3	3.578(16)	N4–C6	1.41(3)
Cs1–O2$^{\#4}$	3.63(3)	N4–C4	1.42(2)
Cs2–O3$^{\#5}$	3.05(2)	N5–C4	1.34(3)
Cs2–N11$^{\#6}$	3.174(18)	N5–C3	1.35(3)
Cs2–N8	3.188(17)	N6–C1	1.31(3)
Cs2–O2	3.352(18)	N6–C5	1.38(3)
Cs2–N13$^{\#7}$	3.357(17)	N7–C6	1.28(2)
Cs2–N9$^{\#7}$	3.378(17)	N7–C5	1.36(3)
Cs2–N7	3.401(17)	N8–C6	1.32(3)
Cs2–O1	3.45(2)	N8–C8	1.35(3)
Cs2–N10	3.474(19)	N9–C7	1.29(3)
Cs2–N12$^{\#8}$	3.53(2)	N9–C8	1.35(2)
Cs3–O1$^{\#2}$	2.998(17)	N10–C7	1.16(3)
Cs3–N5	3.221(17)	N11–C9	1.16(3)
Cs3–N12$^{\#9}$	3.25(2)	N12–C1	1.13(3)
Cs3–N6$^{\#7}$	3.257(18)	N13–C4	1.31(3)
Cs3–N13	3.315(16)	N13–C8	1.36(3)
Cs3–N11$^{\#10}$	3.34(2)		
Cs3–O2$^{\#11}$	3.39(2)		
Cs3–N11	3.49(2)		
Cs3–N7	3.568(16)		

Atom–Atom–Atom	Angle [°]	Atom–Atom–Atom	Angle [°]
C9–N1–C3	118.4(18)	C4–N13–C8	115.7(17)
C2–N2–C5	118.2(18)	N12–C1–N6	175(3)
C2–N3–C3	117.6(17)	N2–C2–N3	121.6(18)
C2–N4–C6	120.2(16)	N2–C2–N4	118.8(18)
C2–N4–C4	120.6(16)	N3–C2–N4	119.5(16)
C6–N4–C4	119.2(16)	N1–C3–N5	116.5(19)
C4–N5–C3	118.1(17)	N1–C3–N3	117.3(19)
C6–N7–C5	119.3(19)	N5–C3–N3	126.1(18)
C6–N8–C8	118.6(18)	N13–C4–N5	120.8(17)
C7–N9–C8	119.9(18)	N13–C4–N4	121.1(17)
N5–C4–N4	118.1(17)	N8–C6–N4	118.5(17)

N2–C5–N7	124.6(19)	N10–C7–N9	173(2)
N2–C5–N6	120(2)	N8–C8–N9	118.4(19)
N7–C5–N6	116(2)	N8–C8–N13	126.8(17)
N7–C6–N8	122.6(19)	N9–C8–N13	114.9(18)
N7–C6–N4	118.8(18)	N11–C9–N1	174(2)

Symmetry transformations used to generate equivalent atoms:

#1: +X, +Y, 1+Z; #2: -0.5+X, 0.5-Y, +Z; #3: -0.5+X, 0.5-Y, 1+Z; #4: -1+X, +Y, 1+Z; #5: +X, +Y, -1+Z; #6: 1.5-X, 0.5+Y, -0.5+Z; #7: 0.5+X, 0.5-Y, +Z; #8: 1-X, 1-Y, -0.5+Z; #9: 1.5-X, -0.5+Y, -0.5+Z; #10: 1-X, -Y, -0.5+Z; #11: 1.5-X, -0.5+Y, 0.5+Z; #12: 0.5+X, 0.5-Y, -1+Z; #13: 1-X, -Y, 0.5+Z; #14: 1.5-X, 0.5+Y, 0.5+Z; #15: 1-X, 1-Y, 0.5+Z; #16: 1+X, +Y, -1+Z;

Table S6. The value of $|\beta|_{avg}$, δ, and Eg for diverse octupolar π-conjugated structures.

Chemical name	anionic group	HOMO-LUMO Gap (eV)	Polarizability anisotropy δ (a. u.)	Averaged first-hyperpolarizability $|\beta|_{avg}$ (a. u.)*
Cyanurate	$[C_3N_3O_3]^{3-}$	6.96	84.26095	1345.554043
Cyamelurate	$[C_6N_7O_3]^{3-}$	5.35	139.57441	2015.239243
Tricyanomelaminate	$[C_3N_3(NCN)_3]^{3-}$	5.64	151.38661	1466.8641
Melonate	$[C_6N_7(NCN)_3]^{3-}$	4.64	253.44150	3341.548281

*The averaged first-order hyperpolarizability ($|\beta|_{avg}$) were calculated using the following equations[20]:

$|\beta|_{avg}=\beta_{J=1} \oplus \beta_{J=3}$ ($\beta_{J=1}$:The contribution of the dipole, $\beta_{J=3}$:The contribution of the octupole)

$\|\beta\|^2=\|\beta_{J=1}\|^2+\|\beta_{J=3}\|^2$

$\|\beta_{J=1}\|^2=\frac{3}{4}[(\beta_{xxx}+\beta_{xyy})^2+(\beta_{yyy}+\beta_{yxx})^2]$

$\|\beta_{J=3}\|^2=\frac{1}{4}[(\beta_{xxx}-3\beta_{xyy})^2+(\beta_{yyy}-3\beta_{yxx})^2]$

Table S7. The SHG response and birefringence of crystals containing large π-conjugated structures.

	Crystal	SHG (×KDP)	Birefringence	Ref.
1	$RbCl{\cdot}(H_3C_3N_3O_3)_2$		0.071[h]	21
2	$RbBr{\cdot}(H_3C_3N_3O_3)_2$		0.075[h]	21
3	$Pb(H_2C_3N_3O_3)(OH)$		0.079[i]	22
4	$Mg(H_2C_3N_3O_3)_2{\cdot}6H_2O$		0.093[h]	23
5	$CsCl{\cdot}(H_3C_3N_3O_3)_2$		0.105[h]	21
6	$CsBr{\cdot}(H_3C_3N_3O_3)$		0.137[h]	24
7	$RbBr{\cdot}(H_3C_3N_3O_3)$		0.138[h]	24
8	$Lu_5(C_3N_3O_3)(OH)_{12}$	4.2	0.148[h]	25
9	$Y_5(C_3N_3O_3)(OH)_{12}$	2.5	0.149[h]	25
10	$Li_2Zn_2(H_2C_3N_3O_3)_2(HC_3N_3O_3)(OH)_2{\cdot}2H_2O$		0.174[i]	26
11	$SrHC_3N_3O_3$		0.184[h]	23
12	$KLi(HC_3N_3O_3){\cdot}2H_2O^{exp}$	5.1	0.186[b]	27
13	$BaZn_2(H_2C_3N_3O_3)_2(HC_3N_3O_3)(OH)_2{\cdot}2H_2O$		0.191[i]	26
14	$K_3Pb(H_2C_3N_3O_3)_5{\cdot}6H_2O$		0.193[c]	28
15	$K_2Sr(H_2C_3N_3S_3)_4{\cdot}5H_2O$		0.194[h]	29
16	$Cs(H_2C_3N_3S_3)$	4.6	0.196[i]	30
17	$Pb(H_2C_3N_3O_3)F$		0.203[i]	22
18	$Ba(H_2C_3N_3O_3)_2{\cdot}8H_2O$	12	0.220[e]	31
19	$RbI{\cdot}(H_3C_3N_3O_3)$		0.227[h]	24
20	$La(H_2C_3N_3O_3)_2{\cdot}(OH){\cdot}2H_2O^{exp}$		0.233[d]	32
21	$Cs_4(HC_3N_3S_3)_2{\cdot}4H_2O$		0.236[h]	33
22	$NaRb_{0.84}Cs_{0.16}(HC_3N_3O_3){\cdot}2H_2O$	3	0.238[c]	34
23	$RbNa(HC_3N_3O_3){\cdot}2H_2O$	5.3	0.239[g]	35
24	$Rb(H_3C_3N_3O_3)(NO_3)$		0.243[h]	36
25	$K_4Cu_3(C_3N_3O_3)_2Br$		0.244[h]	37
26	$Ca(H_2C_3N_3O_3)_2{\cdot}3H_2O$		0.245[h]	23
27	$K_4Cu_3(C_3N_3O_3)_2Cl$		0.249[h]	37
28	$K_2Cd(H_2C_3N_3O_3)_4{\cdot}4H_2O$		0.251[h]	38
29	$\beta\text{-}Sr_3(C_3N_3O_3)_2{\cdot}2H_2O$		0.257[h]	23
30	$LiRb(HC_3N_3O_3){\cdot}2H_2O$	2.7	0.259[d]	34
31	$Gd(H_2C_3N_3O_3)_2{\cdot}(OH){\cdot}5H_2O^{exp}$		0.264[d]	32
32	$Cs_2Zn(H_2C_3N_3O_3)_4{\cdot}4H_2O$		0.264[h]	38
33	$K(H_3C_3N_3O_3)(NO_3)$		0.268[h]	36
34	$Ba(H_2C_3N_3O_3)_2{\cdot}2H_2O$		0.271[h]	23
35	$KBr{\cdot}H_3C_3N_3O_3$		0.273[h]	39
36	$Y(H_2C_3N_3O_3)_2{\cdot}(OH){\cdot}5H_2O^{exp}$		0.274[d]	32
37	$LiCl{\cdot}(H_3C_3N_3O_3)$	d_{22}=4.15	0.280[h]	40
38	$Zn(H_2C_3N_3O_3)_2{\cdot}3H_2O$		0.283[h]	41
39	$Cs_3Na(H_2C_3N_3O_3)_4{\cdot}3H_2O$	0.67	0.290[b]	42

40	$Pb_2Cd(HC_3N_3O_3)_2(OH)_2$		0.291[h]	[43]
41	$Mg(H_2C_3N_3O_3)_2\cdot 8H_2O$		0.293[h]	[23]
42	$NaBr\cdot(H_3C_3N_3O_3))$		0.297[h]	[24]
43	$RbLi(H_2C_3N_3O_3)_2\cdot 2H_2O$		0.300[a]	[44]
44	$CsLi(H_2C_3N_3O_3)_2\cdot 2H_2O$		0.300[a]	[44]
45	$K_2Zn(H_2C_3N_3O_3)_4\cdot 4H_2O$		0.305[h]	[38]
46	$Ba_2Pb(C_3N_3O_3)_2$		0.310[h]	[45]
47	$MgZn_4(OH)_4(C_3N_3O_3)_2$		0.316[a]	[46]
48	$Zn_5(OH)_4(C_3N_3O_3)_2$		0.318[a]	[46]
49	$K_2Pb(H_2C_3N_3O_3)_4\cdot 4H_2O$	2.6	0.325[c]	[28]
50	$Ba_3(C_3N_3O_3)_2$		0.320[h]	[47]
51	$SrHC_3N_3O_3\cdot 2.5H2O$		0.341[h]	[23]
52	$Pb_3(HC_3N_3O_3)_2(OH)_2$		0.342[h]	[43]
53	$Li_2(HC_3N_3O_3)\cdot 2H_2O$		0.345[c]	[34]
54	$Ba_2Ca(C_3N_3O_3)_2$		0.345[h]	[48]
55	$Ba_2Sr(C_3N_3O_3)_2$		0.350[h]	[45]
56	$K_2(HC_3N_3O_3)$		0.350[h]	[49]
57	$Ca_3(C_3N_3O_3)_2$		0.350[f]	[50]
58	$Ba_2Mg(C_3N_3O_3)_2$		0.351[h]	[48]
59	$Rb_2Ca(H_2C_3N_3O_3)_4\cdot 4H_2O$		0.362[h]	[51]
60	$Rb_3Na(H_2C_3N_3O_3)_4\cdot 3H_2O$	0.2	0.368[i]	[52]
61	$K_2Ca(H_2C_3N_3O_3)_4\cdot 4H_2O$		0.371[h]	[51]
62	$K_2Mg(H_2C_3N_3O_3)_4\cdot 4H_2O$		0.376[h]	[51]
63	α−$Sr(H_2C_3N_3O_3)_2\cdot 2H_2O$		0.379[h]	[23]
64	$NaRb_3(H_2C_3N_3O_3)_4\cdot 3H_2O$	0.67	0.389[c]	[34]
65	$Na_2Ba(H_2C_3N_3O_3)_4\cdot 6H_2O$		0.394[h]	[53]
66	$RbNH_4(H_2C_3N_3O_3)_2\cdot 2H_2O$		0.400[i]	[54]
67	$Rb_2(HC_3N_3O_3)$		0.400[c]	[34]
68	$K_2HC_3N_3S_3\cdot 1.5H_2O$		0.400[e]	[55]
69	$GU_3(H_2C_3N_3O_3)_3(H_3C_3N_3O_3)$		0.402[a]	[56]
70	$Li_2Ca(H_2C_3N_3O_3)_4\cdot 6H_2O$		0.407[h]	[53]
71	$GU(H_2C_3N_3O_3)$		0.419[a]	[56]
72	$K_3C_6N_7O_3\cdot 2H_2O$	4	0.446[i]	[57]
73	$Cs_3C_6N_9\cdot H_2O$	9.8	0.520[e]	[58]
74	$Cs_2Mg(H_2C_3N_3S_3)_4\cdot 8H_2O$		0.580[h]	[29]
75	$Cd(H_2C_6N_7O_3)_2\cdot 8H_2O$		0.590[e]	[59]
76	$Cs_3Cl(HC_3N_3S_3)$	11.4	0.600[e]	[60]
77	$NH_4(H_2C_6N_7O_3)\cdot 2H_2O$		0.640[e]	[61]
78	**I**	9	0.619[d]	**This work**
79	**II**	8.7	0.589[d]	**This work**

[a] :@400 nm; [b] :@514 nm; [c] :@532 nm; [d] :@546.1 nm; [e] :@550 nm; [f] :@589.3 nm; [g] :@589.6nm; [h] :@800 nm; [i] :@1064 nm.

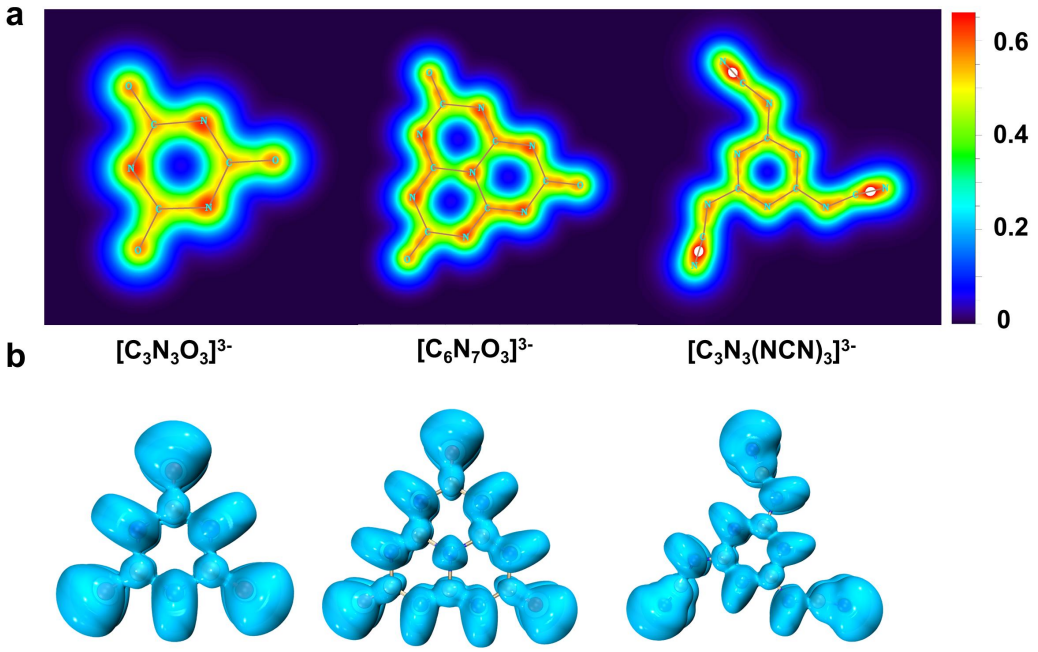

Figure S1. a) LOL-π color-filled map at 1.6 Bohr above the π-conjugated plane and b) ELF-π isosurface for diverse octupolar π-conjugated structures (isovalue = 0.6).

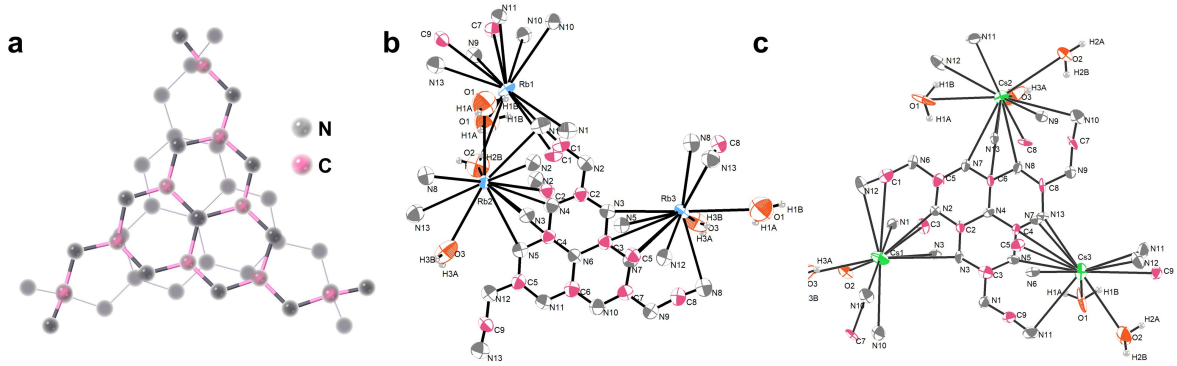

Figure S2. a) Vertical flip of $[C_6N_7(NCN)_3]^{3-}$ group between neighboring layers; The ORTEP diagram (50% probability thermal ellipsoids) for **I** (b) and **II** (c).

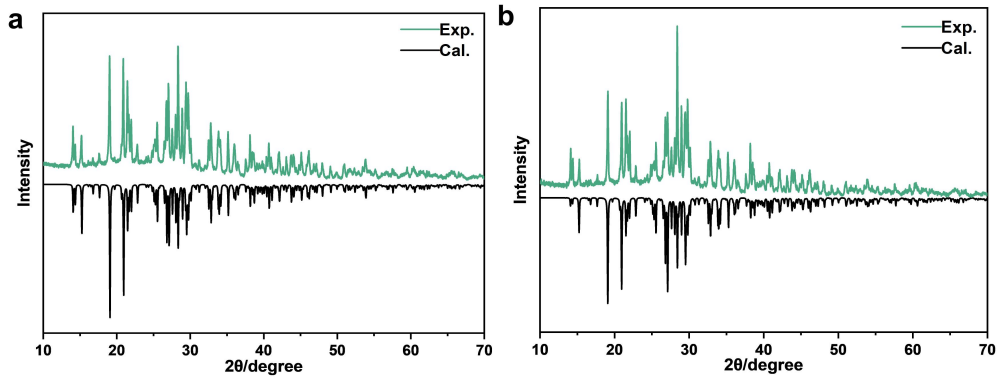

Figure S3. PXRD of a) **I** and b) **II**.

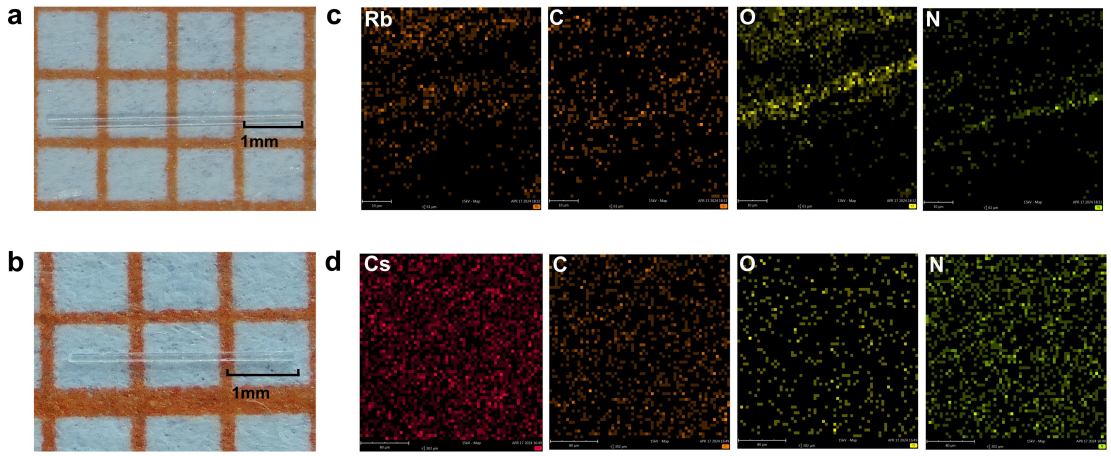

Figure S4. Crystal pictures of a) **I** and b) **II**; Elemental mapping images of c) **I** and d) **II**.

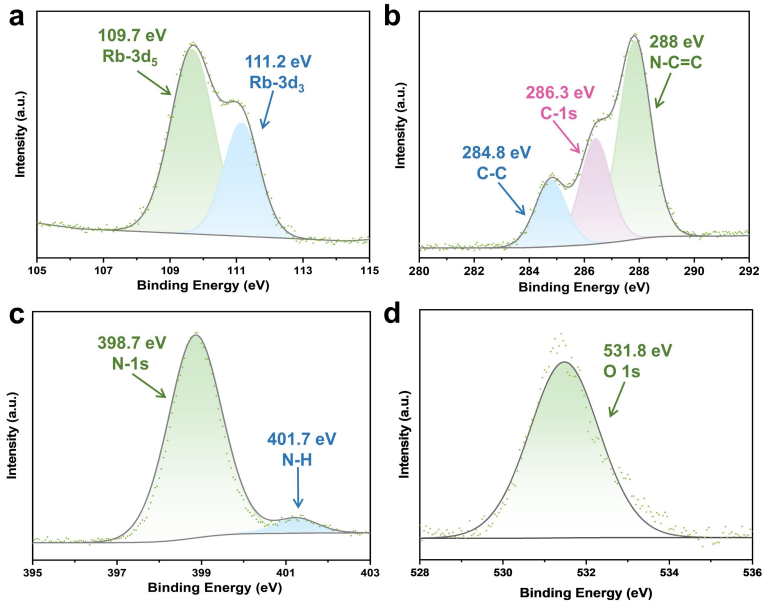

Figure S5. XPS of **I**. a) Rb 3d. b) C 1s. The first peak (284.8 eV) is attributed to C-C from the background, the second peak at 286.3 eV originates from C 1s, and the third peak at 288 eV is attributed to the N-C=N. c) N 1s. The first main peak at 398.8 eV attributed to N 1s and the second peak at 401.4 eV attributed to N-H bonds. d) O 1s. The peak at 531.8 eV comes from the O-H-bonded O in the water of crystallization.

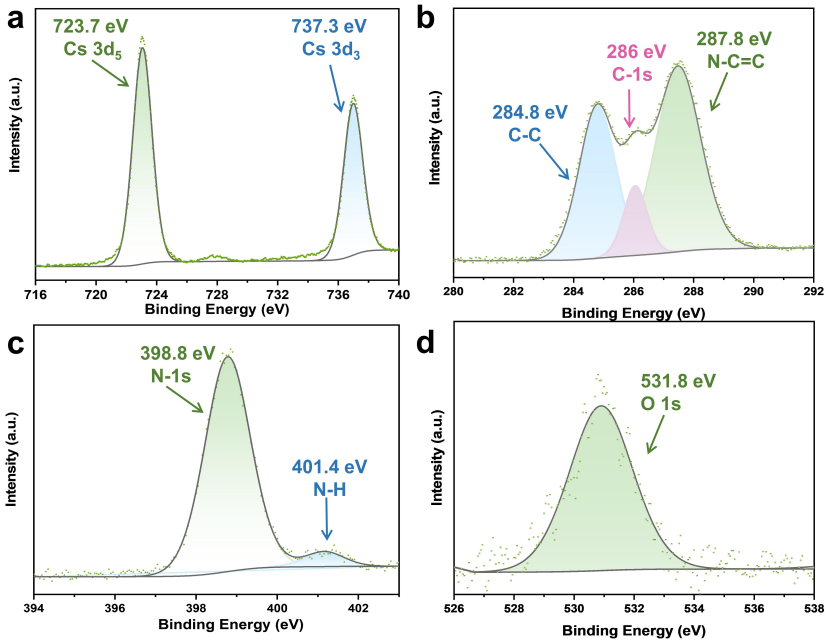

Figure S6. XPS of **II**. a) Cs 3d; b) C 1s; c) N 1s; d) O 1s. For **II**, the attribution of the peaks in the XPS spectra of C 1s, N 1s, and O 1s are very close to those of **I**.

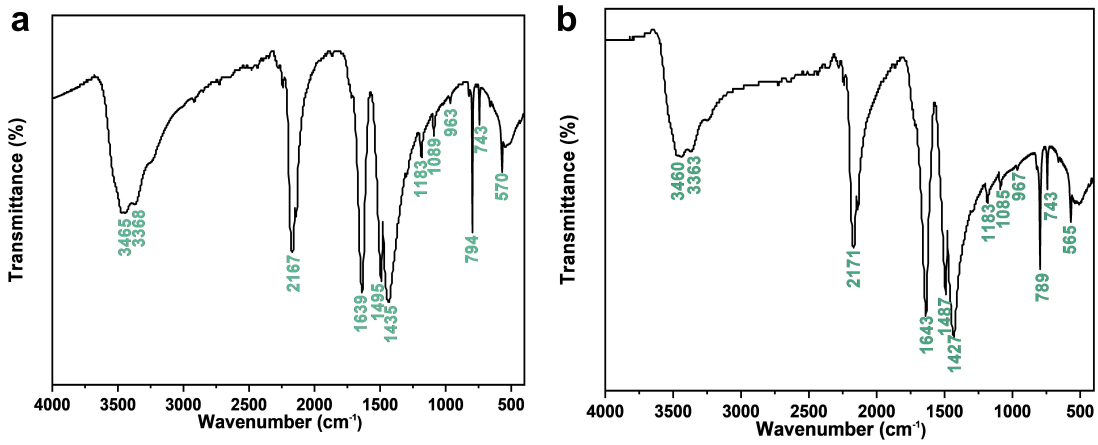

Figure S7. IR spectra of a) **I** and b) **II**. The peak at 3363-3465 cm^{-1} originates from the O-H stretching vibration in the water of crystallization. The characteristic stretching vibrations of the $[C_6N_7]$ ring are shown at 789-794 cm^{-1}, 1183 cm^{-1}, 1427-1435 cm^{-1}, 1487-1495 cm^{-1}, and 1639-1643 cm^{-1}, respectively.[62] The strong absorption peaks at 2167-2171, 1487-1495 cm^{-1} are attributed to the stretching vibration of the side group C≡N[63].

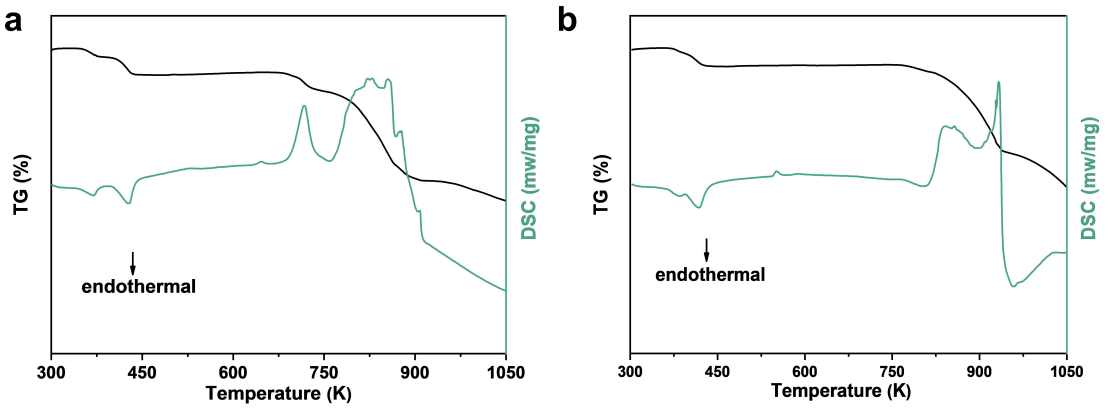

Figure S8. TG-DSC curves of a) **I** and b) **II**. The first and second endothermic peaks correspond to the loss of crystal water, and the subsequent exothermic peaks arise from the decomposition of the $[C_6N_7(NCN)_3]^{3-}$ group. The$[C_6N_7(NCN)_3]^{3-}$ group was found to be thermally stable up to 693 K, but the presence of crystallization water greatly reduced the compounds' decomposition temperature. Therefore, we explored the anhydrous compounds. Pure phase powder of 0.5 g of **I** and **II** with 8 ml of anhydrous ethanol were placed in 23 ml of polytetrafluoroethylene liner, and held at 90 °C for 60 h using the mild hydrothermal method. Unfortunately, the degree of crystallinity of the anhydrous phases were too poor to perform XRD analysis.

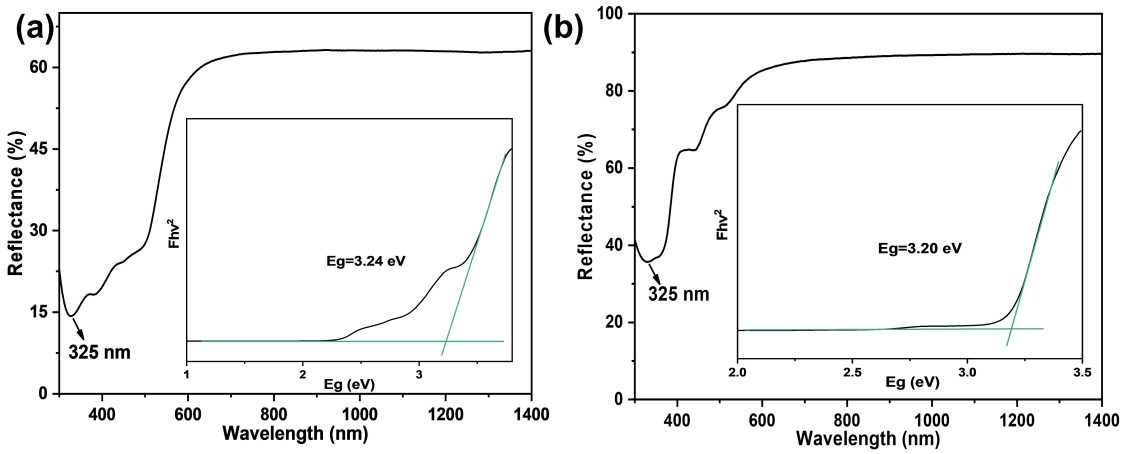

Figure S9. UV−vis−NIR diffuse reflectance spectrum of a) **I** and b) **II**.

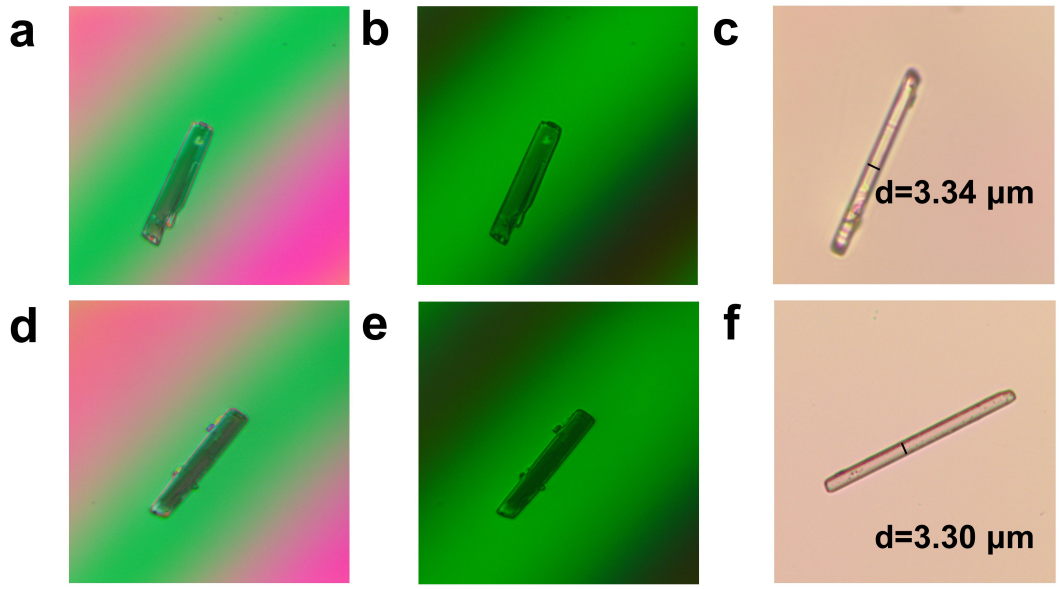

Figure S10. a) The complete extinction of **I** with the right-rotated compensator and b) using the 546 nm filter; c) the measured thickness of **I**. d) The complete extinction of **II** with the right-rotated compensator and e) using the 546 nm filter; f) the measured thickness of **II**.

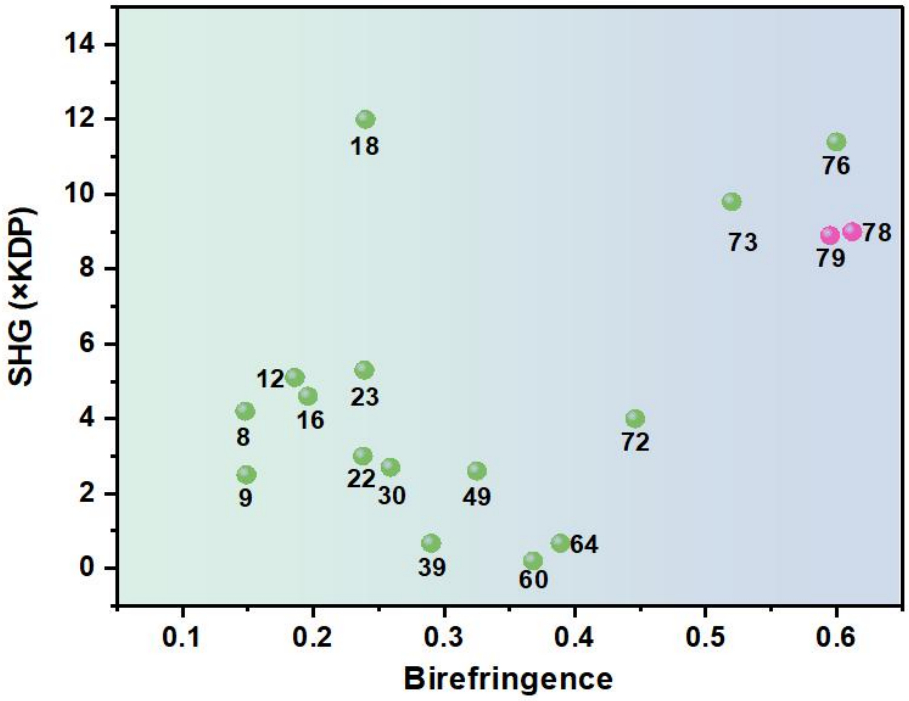

Figure S11. The NLO crystals containing octupolar π-conjugated structures.

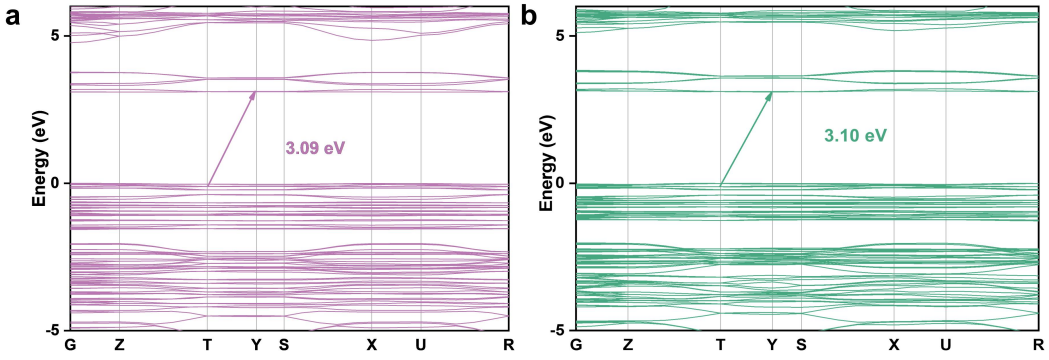

Figure S12. Calculated band structure (GGA method) of a) **I** and b) **II**.

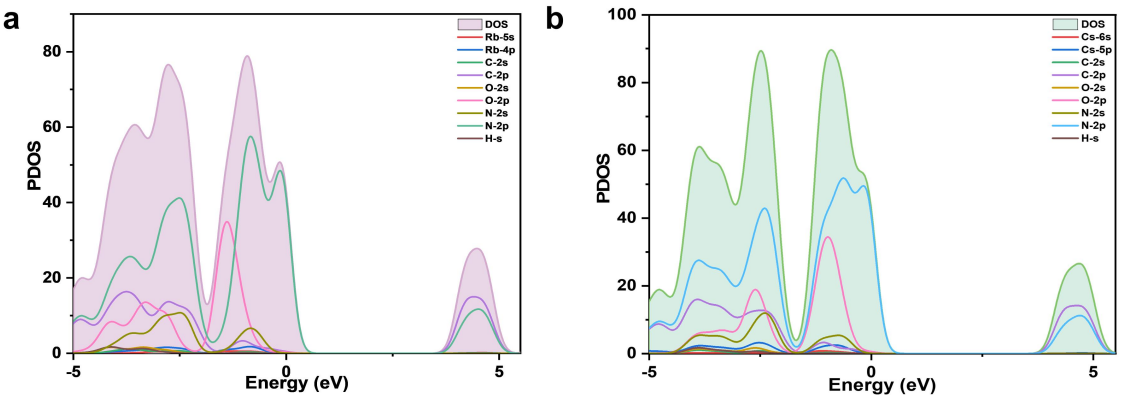

Figure S13. DOS and PDOS a) **I** and b) **II**.

Reference.

1. E. Horvath.Bordon, E. Kroke, I. Svoboda, H. Fuess and R. Riedel, Potassium melonate, $K_3[C_6N_7(NCN)_3]\cdot 5H_2O$, and its potential use for the synthesis of graphite-like C_3N_4 materials, *New J. Chem.*, 2005, **29**, 693-699.
2. SAINT, *Version 7.60A, Bruker analytical X-ray Instruments, inc.,Madison, WI, 2008*.
3. O. V. Dolomanov, L. J. Bourhis, R. J. Gildea, J. A. K. Howard and H. Puschmann, OLEX2: A complete structure solution, refinement and analysis program, *J. Appl. Cryst.* , 2009, **42**, 339–341.
4. G. M. Sheldrick, SHELXT– Integrated space-group and crystal structure determination, *Acta Cryst. A*, 2015, **71**, 3–8.
5. A. L. Spek, Single-crystal structure validation with the program PLATON, *J. Appl. Cryst.*, 2002, **36**, 7-13.
6. Q. Shi, L. Y. Dong and Y. Wang, Evaluating refractive index and birefringence of nonlinear optical crystals: Classical methods and new developments, *Chin. J. Struct. Chem.*, 2023, **42**, 100017.
7. S. K. Kurtz and T. T. Perry, A powder technique for the evaluation of nonlinear optical materials, *J. Appl. Phys.*, 1968, **39**, 3798–3813.
8. M. J. T. Frisch, G. W.; Schlegel, H. B.; Scuseria, G. E.; Robb, M. A.; Cheeseman, J. R.; Scalmani, G.; Barone, V.; Mennucci, B.; Petersson, G. A.; Nakatsuji, H.; Caricato, M.; Li, X.; Hratchian, H. P.; Izmaylov, A. F.; Bloino, J.; Zheng, G.; Sonnenberg, J. L.; Hada, M.; Ehara, M.; Toyota, K.; Fukuda, R.; Hasegawa, J.; Ishida, M.; Nakajima, T.; Honda, Y.; Kitao, O.; Nakai, H.; Vreven, T.; Montgomery, J. A., Jr.; Peralta, J. E.; Ogliaro, F.; Bearpark, M.; Heyd, J. J.; Brothers, E.; Kudin, K. N.; Staroverov, V. N.; Kobayashi, R.; Normand, J.; Raghavachari, K.; Rendell, A.; Burant, J. C.; Iyengar, S. S.; Tomasi, J.; Cossi, M.; Rega, N.; Millam, J. M.; Klene, M.; Knox, J. E.; Cross, J. B.; Bakken, V.; Adamo, C.; Jaramillo, J.; Gomperts, R.; Stratmann, R. E.; Yazyev, O.; Austin, A. J.; Cammi, R.; Pomelli, C.; Ochterski, J. W.; Martin, R. L.; Morokuma, K.; Zakrzewski, V. G.; Voth, G. A.; Salvador, P.; Dannenberg, J. J.; Dapprich, S.; Daniels, A. D.; Farkas, Ö.; Foresman, J. B.; Ortiz, J. V.; Cioslowski, J.; Fox, D. J. , Gaussian 09, *Gaussian, Inc., Wallingford CT*, 2009.
9. T. Lu and F. W. Chen, Multiwfn: A multifunctional wavefunction analyzer, *J. Comput. Chem.*, 2012, **33**, 580-592.
10. W. Humphrey, A. Dalke and K. Schulten, VMD: Visual molecular dynamics, *J. Mol. Graph.*, 1996, **14**, 33-38.
11. M. D. Segall, J. D. L. Philip, M. J. Probert, C. J. Pickard, P. J. Hasnip, S. J. Clark and M. C. Payne, First-principles simulation: ideas, illustrations and the CASTEP code, *J. Condens. Matter. Phys.*, 2002, **14**, 2717.
12. J. P. Perdew, K. Burke and M. Ernzerhof, Generalized gradient aproximation made simple, *Phys. Rev. Lett.*, 1996, **77**, 3865–3868.
13. J. S. Lin, A. Qteish, M. C. Payne and V. Heine, Optimized and transferable nonlocal separable *ab* initio pseudopotentials, *Phys. Rev. B*, 1993, **47**, 4174–4180.
14. A. M. Rappe, K. M. Rabe, E. Kaxiras and J. D. Joannopoulos, Optimized pseudopotentials, *Phys. Rev. B*, 1990, **41**, 1227–1230.

15. A. V. Krukau, O. A. Vydrov, A. F. Izmaylov and G. E. Scuseria, Influence of the exchange screening parameter on the performance of screened hybrid functionals, *J. Chem. Phys.*, 2006, **125**, 224106.
16. Z. S. Lin, X. X. Jiang, L. Kang, P. F. Gong, S. Y. Luo and M. H. Lee, First-principles materials applications and design of nonlinear optical crystals, *J. Phys. D Appl. Phys.*, 2014, **47**, 253001.
17. C. Aversa and J. E. Sipe, Nonlinear optical susceptibilities of semiconductors: results with a length-gauge analysis, *Phys. Rev. B*, 1995, **52**, 14636–14645.
18. S. N. Rashkeev, W. R. L. Lambrecht and B. Segall, Efficient *ab* initio method for the calculation of frequency-dependent second-order optical response in semiconductors, *Phys. Rev. B*, 1998, **57**, 3905–3919.
19. M. H. Lee, C. H. Yang and J. H. Jan, Band-resolved analysis of nonlinear optical properties of crystalline and molecular materials, *Phys. Rev. B*, 2004, **70**, 235110.
20. J. Zyss and I. Ledoux, Nonlinear optics in multipolar media theory and experiments, *Chem. Rev.*, 1994, **94**, 77-105.
21. J. H. Wang, X. Y. Zhang, F. Liang, Z. G. Hu and Y. C. Wu, Synthesis and characterization of new-type ionic cocrystals with cyanuric acid and alkali halides: $AX{\cdot}(H_3C_3N_3O_3)_2$ (A = Rb, Cs; X = Cl, Br), *Cryst. Growth. Des.*, 2021, **21**, 7194-7200.
22. Y. Chen, C. L. Hu, Z. Fang, Y. L. Li and J. G. Mao, From $Pb(H_2C_3N_3O_3)(OH)$ to $Pb(H_2C_3N_3O_3)F$: homovalent anion substitution-induced band gap enlargement and birefringence enhancement, *Inorg. Chem.*, 2022, **61**, 1778-1786.
23. X. H. Meng, K. J. Kang, F. Liang, J. Tang, W. L. Yin, Z. S. Lin and M. Xia, Optimal arrangement of π-conjugated anionic groups in hydro-isocyanurates leads to large optical anisotropy and second-harmonic generation effect, *Inorg. Chem. Front.*, 2020, **7**, 3674-3686.
24. J. H. Wang, X. Y. Zhang, F. Liang, Z. G. Hu and Y. C. Wu, Co-crystal $AX{\cdot}(H_3C_3N_3O_3)$ (A = Na, Rb, Cs; X = Br, I): a series of strongly anisotropic alkali halide cyanurates with a planar structural motif and large birefringence, *Dalton. Trans.*, 2021, **50**, 11555-11561.
25. X. H. Meng, X. Y. Zhang, Q. X. Liu, Z. Y. Zhou, X. X. Jiang, Y. G. Wang, Z. S. Lin and M. J. Xia, Perfectly encoding pi-conjugated anions in the $RE_5(C_3N_3O_3)(OH)_{12}$ (RE=Y, Yb, Lu) family with strong second harmonic generation response and balanced birefringence, *Angew. Chem. Int. Ed.*, 2023, **62**, e202214848.
26. D. D. Wang, F. Liang, X. Y. Zhang, Z. G. Hu and Y. C. Wu, The first positive uniaxial cyanurate crystals containing a crown-like anionic group arrangement and strengthened optical anisotropy, *Cryst. Growth. Des.*, 2021, **21**, 2348-2354.
27. D. H. Lin, M. Luo, C. S. Lin, F. Xu and N. Ye, $KLi(HC_3N_3O_3){\cdot}2H_2O$: Solvent-drop grinding method toward the hydro-isocyanurate nonlinear optical crystal, *J. Am. Chem. Soc*, 2019, **141**, 3390-3394.
28. Y. Chen, C. L. Hu, Z. Fang and J. G. Mao, $K_2Pb(H_2C_3N_3O_3)_4(H_2O)_4$: a potential UV nonlinear optical material with large birefringence, *Inorg. Chem. Front.*, 2021, **8**, 3547-3555.
29. X. Hao, C. S. Lin, M. Luo, Y. Q. Zhou, N. Ye and E. Shangguan, $Cs_2Mg(H_2C_3N_3S_3)_4{\cdot}8H_2O$: An excellent birefringent material with giant optical anisotropy in π-conjugated trithiocyanurate, *Inorg. Chem.*, 2023, **62**, 7611-7616.

30. X. Hao, C. S. Lin, N. Ye, D. H. Lin, D. Zhao, Y. Q. Zhou, E. Shangguan and M. Luo, Explorations of second-order nonlinear optical materials in the monovalent trithiocyanurate system, *Cryst. Growth. Des.*, 2022, **23**, 362-368.
31. Y. Q. Li, W. Q. Huang, Y. Zhou, X. Y. Song, J. Y. Zheng, H. Wang, Y. P. Song, M. J. Li, J. H. Luo and S. G. Zhao, A high-performance nonlinear optical crystal with a building block containing expanded π-delocalization, *Angew. Chem. Int. Ed.*, 2022, **62**, e202215145.
32. X. Hao, M. Luo, C. S. Lin, D. H. Lin, L. J. Cao and N. Ye, $RE(H_2C_3N_3O_3)_2\cdot(OH)\cdot xH_2O$ (RE = La, Y and Gd): potential UV birefringent materials with strong optical anisotropy originating from the $(H_2C_3N_3O_3)^-$ group, *Dalton. Trans.*, 2019, **48**, 12296-12302.
33. J. M. Zhao, H. K. Liu, X. D. Zhang, B. B. Zhang and Y. Wang, Facile synthesis of cesium trithiocyanurate with high ionic conductivity and large birefringence properties, *CrystEngComm*, 2020, **22**, 6495-6501.
34. J. Lu, Y. K. Lian, L. Xiong, Q. R. Wu, M. Zhao, K. X. Shi, L. Chen and L. M. Wu, How to maximize birefringence and nonlinearity of pi-conjugated cyanurates, *J. Am. Chem. Soc.*, 2019, **141**, 16151-16159.
35. Y. X. Song, D. H. Lin, M. Luo, C. S. Lin, Q. L. Chen and N. Ye, $RbNa(HC_3N_3O_3)\cdot 2H_2O$ exhibiting a strong second harmonic generation response and large birefringence as a new potential UV nonlinear optical material, *Inorg. Chem. Front.*, 2020, **7**, 150-156.
36. X. Hao, M. Luo, C. S. Lin, G. Peng, T. Yan, D. H. Lin, L. L. Cao, X. F. Long, G. S. Yang and N. Ye, $A(H_3C_3N_3O_3)(NO_3)$ (A = K, Rb): Alkali-metal nitrate isocyanurates with strong optical anisotropy, *Inorg. Chem.*, 2020, **59**, 10361-10367.
37. K. J. Kang, F. Liang, X. H. Meng, J. Tang, T. X. Zeng, M. J. Xia, Z. S. Lin, W. L. Yin and K. Bin, $K_4Cu_3(C_3N_3O_3)_2X$ (X = Cl, Br): strong anisotropic layered semiconductors containing mixed p-p and d-p conjugated pi-bonds, *Chem. Commun.*, 2020, **56**, 12534-12537.
38. K. J. Kang, X. H. Meng, F. Liang, J. Tang, T. X. Zeng, W. L. Yin, Z. S. Lin and M. J. Xia, Hydroisocyanurates $X_2Y(H_2C_3N_3O_3)_4\cdot 4H_2O$ (X = K, Cs; Y = Zn, Cd) with large birefringence stemming from π-conjugated $(H_2C_3N_3O_3)^-$anions, *CrystEngComm*, 2020, **22**, 2128-2131.
39. X. H. Meng, K. J. Kang, Y. Q. Liu, J. Tang, X. X. Jiang, W. L. Yin, Z. S. Lin and M. J. Xia, Mechanochemical synthesis of an ionic cocrystal with large birefringence resulting from neutral planar π-conjugated groups, *Cryst. Growth. Des.*, 2020, **20**, 7588-7592.
40. F. Liang, N. Z. Wang, X. M. Liu, Z. S. Lin and Y. C. Wu, Co-crystal $LiCl\cdot(H_3C3N_3O_3)$: a promising solar-blind nonlinear optical crystal with giant nonlinearity from coplanar π-conjugated groups, *Chem. Commun.*, 2019, **55**, 6257-6260.
41. D. D. Wang, X. Y. Zhang, F. Liang, Z. G. Hu and Y. C. Wu, $Zn(H_2C_3N_3O_3)_2\cdot 3H_2O$: the first single-$d^{10}$ transition metal based ultraviolet hydroisocyanurate crystal with large birefringence, *Dalton. Trans.*, 2021, **50**, 5617-5623.
42. X. H. Meng, F. Liang, J. Tang, K. J. Kang, Q. Huang, W. L. Yin, Z. S. Lin and M. J. Xia, $Cs_3Na(H_2C_3N_3O_3)_4\cdot 3H_2O$: A mixed alkali-metal hydroisocyanurate nonlinear optical material containing π-conjugated six-membered-ring units, *Eur. J. Inorg. Chem.*, 2019, **2019**, 2789-2789.
43. X. H. Meng, K. J. Kang, F. Liang, J. Tang, Z. S. Lin, W. L. Yin and M. J. Xia, "Old dog, new tricks": the lone pair effect inducing divergent optical responses in lead cyanurates containing pi-bonds, *Dalton. Trans.*, 2020, **49**, 1370-1374.

44. X. H. Meng, F. Liang, J. Tang, K. J. Kang, T. X. Zeng, W. L. Yin, R. X. Guo, Z. S. Lin and M. J. Xia, Parallel alignment of pi-conjugated anions in hydroisocyanurates enhancing optical anisotropy, *Inorg. Chem.*, 2019, **58**, 8948-8952.
45. K. J. Kang, F. Liang, X. H. Meng, J. Tang, T. X. Zeng, W. L. Yin, M. J. Xia, Z. S. Lin and B. Kang, $Ba_2M(C_3N_3O_3)_2$ (M = Sr, Pb): Band engineering from p-pi interaction via homovalent substitution in metal cyanurates containing planar pi-conjugated groups, *Inorg. Chem.*, 2019, **58**, 9553-9556.
46. X. M. Liu, P. F. Gong and Z. S. Lin, $AZn_4(OH)_4(C_3N_3O_3)_2$ (A = Mg, Zn): Two Zn-based cyanurate crystals with various cation coordination and large birefringence, *Inorg. Chem.*, 2021, **60**, 10890-10894.
47. J. Tang, F. Liang, X. H. Meng, K. J. Kang, W. L. Yin, T. X. Zeng, M. J. Xia, Z. S. Lin, J. Y. Yao, G. C. Zhang and B. Kang, $Ba_3(C_3N_3O_3)_2$: A new phase of barium cyanurate containing parallel π-conjugated groups as a birefringent material replacement for calcite, *Cryst. Growth. Des.*, 2018, **19**, 568-572.
48. Z. Li, F. Liang, Y. W. Guo, Z. S. Lin, J. Y. Yao, G. C. Zhang, W. L. Yin, Y. C. Wu and C. T. Chen, $Ba_2M(C_3N_3O_3)_2$ (M = Mg, Ca): potential UV birefringent materials with strengthened optical anisotropy originating from the $(C_3N_3O_3)^{3-}$ group, *J. Mater. Chem. C*, 2018, **6**, 12879-12887.
49. N. Z. Wang, F. Liang, Y. Yang, S. Z. Zhang and Z. S. Lin, A new ultraviolet transparent hydra-cyanurate $K_2(C_3N_3O_3H)$ with strong optical anisotropy from delocalized pi-bonds, *Dalton. Trans.*, 2019, **48**, 2271-2274.
50. M. Kalmutzki, M. Ströbele, F. Wackenhut, A. J. Meixner and H. J. Meyer, Synthesis, structure, and frequency-doubling effect of calcium cyanurate, *Angew. Chem. Int. Ed.*, 2014, **53**, 14260-14263.
51. X. H. Meng, F. Liang, K. J. Kang, J. Tang, Q. Huang, W. L. Yin, Z. S. Lin and M. J. Xia, A rich structural chemistry in pi-conjugated hydroisocyanurates: layered structures of $A_2B(H_2C_3N_3O_3)_4{\cdot}nH_2O$ (A = K, Rb, Cs; B = Mg, Ca; n = 4, 10) with high ultraviolet transparency and strong optical anisotropy, *Dalton. Trans.*, 2019, **48**, 9048-9052.
52. M. Aibibula, L. Wang and S. Huang, $Rb_3Na(H_2C_3N_3O_3)_4{\cdot}3H_2O$ with large birefringence, *ACS Omega*, 2019, **4**, 22197-22202.
53. X. H. Meng, F. Liang, J. Tang, K. J. Kang, W. L. Yin, T. X. Zeng, B. Kang, Z. S. Lin and M. J. Xia, LiO_4 tetrahedra lock the alignment of π-conjugated layers to maximize optical anisotropy in metal hydroisocyanurates, *Inorg. Chem. Front.*, 2019, **6**, 2850-2854.
54. M. Aibibula and L. Wang, A UV birefringent crystal: $RbNH_4(H_2C_3N_3O_3)_2{\cdot}2H_2O$, *Inorg. Chem. Commun.*, 2020, **120**.
55. Y. P. Song, W. Q. Huang, Y. Zhou, Y. Q. Li, Q. T. Xu, H. Wang, M. J. Li, X. J. Kuang, J. H. Luo and S. G. Zhao, α-BBO-like π-conjugated crystal with large birefringence, *Cryst. Growth. Des.*, 2023, **23**, 1330-1335.
56. X. M. Liu, L. Kang, R. X. Guo and Z. S. Lin, Two metal-free cyanurate crystals with a large optical birefringence resulting from the combination of π-conjugated units, *Dalton. Trans.*, 2021, **50**, 17495-17498.
57. X. Y. Zhang, X. G. Du, J. H. Wang, F. Y. Wang, F. Liang, Z. G. Hu, Z. S. Lin and Y. C. Wu, $K_3C_6N_7O_3{\cdot}2H_2O$: A multifunctional nonlinear optical cyamelurate crystal with colossal π-conjugated orbitals, *ACS Appl. Mater.*, 2022, **14**, 53074-53080.

58. Y. Q. Li, Q. C. Wu, Z. S. Lin, Y. C. Liu, Y. Zhou, X. Chen, M. J. Li, M. C. Hong, J. H. Luo and S. G. Zhao, Maximizing the linear and nonlinear optical responses of alkaline tricyanomelaminate, *Fundam. Res.*, 2023, **3**, 974-978.
59. Y. Q. Li, X. Zhang, J. Y. Zheng, Y. Zhou, W. Q. Huang, Y. P. Song, H. Wang, X. Y. Song, J. H. Luo and S. G. Zhao, A hydrogen bonded supramolecular framework birefringent crystal, *Angew. Chem. Int. Ed.*, 2023, **62**, e202304498.
60. M. J. Li, X. Zhang, Z. Y. Xiong, Y. Q. Li, Y. Zhou, X. Chen, Y. P. Song, M. C. Hong, J. H. Luo and S. G. Zhao, A hybrid antiperovskite with strong linear and second-order nonlinear optical responses, *Angew. Chem. Int. Ed.*, 2022, **61**, e202211151.
61. Y. Q. Li, Y. Zhou, B. Ahmed, Q. T. Xu, W. Q. Huang, Y. P. Song, X. Y. Song, B. Chen, J. H. Luo and S. G. Zhao, A highly birefringent metal-free crystal assembled by cooperative non-covalent interactions, *Mater. Horiz.*, 2024, DOI: 10.1039/d4mh00422a.
62. B. Jürgens, E. Irran, J. Senker, P. Kroll, Helen Müller and W. Schnick, Melem (2,5,8-Triamino-tri-s-triazine), an important intermediate during condensation of melamine rings to graphitic carbon nitride: synthesis, structure determination by x-ray powder diffractometry, solid-state nmr, and theoretical studies, *J. Am. Chem. Soc.*, 2003, **125**, 10288-10300.
63. S. J. Makowski and W. Schnick, $Rb_3[C_6N_7(NCN)_3]\cdot 3H_2O$ and $Cs_3[C_6N_7(NCN)_3]\cdot 3H_2O$ – Synthesis, crystal structure and thermal behavior of two novel alkali melonates, *Z. Anorg. Allg. Chem.*, 2009, **635**, 2197-2202.